Magnetization process of atacamite: a case of weakly coupled $S = 1/2$ sawtooth chains – Supplemental Material –

L. Heinze,[1] H. O. Jeschke,[2] I. I. Mazin,[3,4] A. Metavitsiadis,[5] M. Reehuis,[6] R. Feyerherm,[6] J.-U. Hoffmann,[6] M. Bartkowiak,[6] O. Prokhnenko,[6] A. U. B. Wolter,[7] X. Ding,[8] V. S. Zapf,[8] C. Corvalán Moya,[8] F. Weickert,[8] M. Jaime,[8] K. C. Rule,[9] D. Menzel,[1] R. Valentí,[10] W. Brenig,[5] and S. Süllow[1]

[1] *Institut für Physik der Kondensierten Materie, TU Braunschweig, D-38106 Braunschweig, Germany*
[2] *Research Institute for Interdisciplinary Science, Okayama University, Okayama 700-8530, Japan*
[3] *Department of Physics and Astronomy, George Mason University, Fairfax, Virginia 22030, USA*
[4] *Quantum Science and Engineering Center, George Mason University, Fairfax, Virginia 22030, USA*
[5] *Institut für Theoretische Physik, TU Braunschweig, D-38106 Braunschweig, Germany*
[6] *Helmholtz-Zentrum Berlin für Materialien und Energie GmbH, D-14109 Berlin, Germany*
[7] *Institute for Solid State and Materials Research, Leibniz IFW Dresden, D-01069 Dresden, Germany*
[8] *National High Magnetic Field Laboratory, Los Alamos National Laboratory, Los Alamos, New Mexico 87545, USA*
[9] *Australian Centre for Neutron Scattering, Australian Nuclear Science and Technology Organisation, Lucas Heights, NSW 2234, Australia*
[10] *Institut für Theoretische Physik, Goethe-Universität Frankfurt, D-60438 Frankfurt am Main, Germany*

In this Supplementary Material we present additional information on the characterization of the atacamite single crystals and the neutron diffraction experiments for crystal and magnetic structure determination. Further, we provide additional information on the electronic structure calculations as well as the classical mean field theory of an individual Δ-chain and a collection of chains. We also present additional experimental data probing the metamagnetic transition and theoretical results for a sawtooth chain with additional in-chain coupling as well as ED results for the Δ-chain.

SINGLE CRYSTAL MATERIAL AND CRYSTAL STRUCTURE

For this study we have investigated various single crystalline natural specimens of atacamite, $Cu_2Cl(OH)_3$. Most of the crystals studied here have been obtained from a batch found in the Moonta Mines and the Poona Mine, Moonta, South Australia, Australia. In addition, a smaller batch was obtained from La Farola Mine, Tierra Amarilla, Atacama, Chile. Where necessary, the crystals were removed from the matrix. Subsequently, the material was broadly characterized with respect to single crystallinity by X-ray diffraction and the magnetic properties by susceptibility measurements. Regarding the magnetic properties, no significant sample dependence could be detected. In addition, in the neutron diffraction experiments, aside from the magnetic studies, a full crystal structure refinement was performed.

EXPERIMENTAL DETAILS: NEUTRON SCATTERING

For the single-crystal and magnetic structure refinement, neutron diffraction experiments were carried out on the four-circle diffractometer E5 at the BER II reactor of the Helmholtz-Zentrum Berlin für Materialien und Energie. This instrument uses a Cu monochromator selecting the neutron wavelength $\lambda = 0.896$ Å. Data sets of Bragg reflections were collected with a two-dimensional position-sensitive ^{3}He-detector, $90 \times 90\,\mathrm{mm}^2$ (32×32 pixels). The crystal structure refinements were carried out using the program *Xtal* 3.4 [S1]. The nuclear scattering lengths $b(\mathrm{H}) = -3.7409\,\mathrm{fm}$, $b(\mathrm{O}) = 5.805\,\mathrm{fm}$, $b(\mathrm{Cl}) = 9.5792\,\mathrm{fm}$ and $b(\mathrm{Cu}) = 7.718\,\mathrm{fm}$ were used [S2]. For the absorption correction (Gaussian integration) we used the absorption coefficient $\mu = 0.160\,\mathrm{cm}^{-1}$. Secondary extinction has been corrected using the formalism of Zachariasen (type I). Extinction is dominated by the mosaic spread (sometimes referred to as *secondary extinction*). The refinable extinction parameter g is related to the mosaic distribution function. For the investigation of the magnetic structure we used the longer wavelength $\lambda = 2.39$ Å at E5. The magnetic form factor of the Cu^{2+} ion was taken from Ref. [S3].

Magnetic field dependent neutron diffraction experiments on the magnetically ordered phase of atacamite were carried out using the flat-cone diffractometer E2 at the BER II reactor of the Helmholtz-Zentrum Berlin. These studies were carried out analogous to those presented in Ref. [S4] (neutron wavelength $\lambda = 2.38$ Å), with the intensity of the magnetic Bragg peak $(1/2\ 0\ 1/2)_\mathrm{M}$ monitored in a magnetic field $\mathbf{H} \parallel b$ axis up to 6.5 T.

An additional field-dependent neutron scattering experiment has been performed at the High Magnetic Field Facility for Neutron Scattering of the Helmholtz-Zentrum Berlin in fields up to 25 T. The facility consists of a continuous-field hybrid magnet, the High-Field Magnet (HFM), providing the time-of-flight Extreme Environment Diffractometer

(EXED) with a horizontal magnetic field. Neutron scattering can be detected within an opening angle of the magnet of ±30° in both forward and backward scattering geometry. For the experiment described in this paper, the forward scattering geometry was used. In order to increase the accessible neutron scattering angle, the whole magnet was rotated by $\omega_{\mathrm{magnet}} = -12°$ away from the incident beam direction. A wavelength band of 0.7 – 2.9 Å was used for the experiment. The sample was aligned with $\mathbf{H} \parallel b$ axis with the c axis lying within the horizontal plane as well. This way, we were able to detect the $(\overline{1/2}\ 0\ \overline{1/2})_{\mathrm{M}}$ reflection and measure its intensity as function of field and temperature.

EXPERIMENTAL RESULTS: CRYSTAL STRUCTURE

In order to investigate the crystal structure of atacamite, $Cu_2Cl(OH)_3$, a single-crystal data set has been collected at 295 K using the instrument E5 at Helmholtz-Zentrum Berlin. Two needle-shaped mineral samples I ($m = 39.0$ mg, used for the E2 experiments) and II ($m = 41.1$ mg, used for the HFM/EXED experiment) with the dimensions $2 \times 6 \times 2\,\mathrm{mm}^3$ have been used. In agreement with an earlier study [S5], the crystal structure could be successfully refined in the orthorhombic space group *Pnma* (No. 62). In this structure the heavier atoms were found to be at the following Wyckoff positions: Cu(1) at $2a(0,0,0)$, Cu(2), Cl, O(1) at $4c(x,1/4,z)$, and O(2) at $8d(x,y,z)$. For the crystal structure refinements, we have used the positional parameters of these atoms given in Ref. [S5] as starting values. As well, the lattice parameters have been taken from Ref. [S5], with $a = 6.02797(11)$ Å, $b = 6.86383(13)$ Å and

Single crystal I (Poona Mine, Moonta, South Australia, Australia)

Atom	Site	x	y	z	U_{11}	U_{22}	U_{33}	U_{12}	U_{13}	U_{23}	Occ.
Cu(1)	4*a*	0	0	0	0.78(6)	0.80(6)	0.66(3)	−0.15(5)	0.18(5)	−0.20(5)	1
Cu(2)	4*c*	0.1907(3)	1/4	0.2553(2)	0.42(6)	0.77(6)	0.79(6)	0	−0.22(5)	0	1
Cl	4*c*	0.3518(3)	3/4	0.0559(2)	0.89(6)	1.19(6)	1.28(6)	0	−0.18(5)	0	1
O(1)	4*c*	0.1515(4)	1/4	−0.0036(3)	0.75(9)	0.67(8)	1.27(9)	0	0.09(8)	0	1
O(2)	8*d*	0.4416(3)	0.0653(2)	0.2881(2)	0.98(7)	0.52(6)	0.68(6)	−0.04(5)	−0.14(5)	−0.01(5)	1
H(1)	4*c*	0.7019(9)	3/4	0.0418(6)	1.79(23)	2.80(23)	3.00(25)	0	1.10(20)	0	1
H(2)	8*d*	0.4285(6)	0.5479(5)	0.2243(4)	2.97(17)	1.42(12)	2.53(16)	−0.10(12)	−0.18(14)	−0.98(12)	1

Bond length (Å)		Bond angle (°)	
d[Cu(1)–O(1)]	1.9442(11)	Cu(1)–O(1)–Cu(1)	123.91(13)
d[Cu(1)–O(2)]	2.0136(17)	Cu(1)–O(2)–Cu(2)	101.50(9)
d[Cu(2)–O(2)]	1.9961(21)	Cu(2)–O(2)–Cu(2)	97.84(8)
d[Cu(2)–O(2)]	2.0044(21)	Cu(1)–O(2)–Cu(2)	114.70(9)
d[O(1)–H(1)]	0.950(6)		
d[O(2)–H(2)]	0.974(4)		

Single crystal II (Moonta Mines, Moonta, South Australia, Australia)

Atom	Site	x	y	z	U_{11}	U_{22}	U_{33}	U_{12}	U_{13}	U_{23}	Occ.
Cu(1)	4*a*	0	0	0	0.91(4)	0.52(5)	0.75(3)	−0.02(3)	0.14(3)	−0.15(4)	1
Cu(2)	4*c*	0.1905(2)	1/4	0.2554(1)	0.55(4)	0.58(5)	0.95(4)	0	−0.22(5)	0	1
Cl	4*c*	0.3514(1)	3/4	0.0557(1)	0.94(3)	0.98(4)	1.32(6)	0	−0.21(3)	0	1
O(1)	4*c*	0.1501(2)	1/4	−0.0021(2)	0.87(5)	0.67(5)	1.17(5)	0	0.07(5)	0	1
O(2)	8*d*	0.4414(2)	0.0653(2)	0.2883(2)	0.84(4)	0.52(4)	0.85(3)	−0.07(3)	−0.11(3)	−0.08(3)	1
H(1)	4*c*	0.6982(5)	3/4	0.0418(4)	1.71(11)	2.51(15)	4.02(16)	0	1.55(12)	0	1
H(2)	8*d*	0.4278(4)	0.5479(3)	0.2246(3)	2.99(10)	2.00(10)	2.57(10)	−0.19(7)	−0.23(8)	−0.97(7)	1

Bond length (Å)		Bond angle (°)	
d[Cu(1)–O(1)]	1.9399(6)	Cu(1)–O(1)–Cu(1)	124.39(7)
d[Cu(1)–O(2)]	2.0123(10)	Cu(1)–O(2)–Cu(2)	101.51(5)
d[Cu(2)–O(2)]	1.9961(13)	Cu(2)–O(2)–Cu(2)	97.80(5)
d[Cu(2)–O(2)]	2.0056(13)	Cu(1)–O(2)–Cu(2)	114.75(6)
d[O(1)–H(1)]	0.983(3)		
d[O(2)–H(2)]	0.973(2)		

TABLE SI. Result of a crystal structure refinement of atacamite, $Cu_2Cl(OH)_3$, for two single crystalline specimens using single-crystal neutron diffraction data collected at 295 K. The anisotropic thermal parameters U_{ij} (given in 100Å^2) are in the form $\exp\left[-2\pi^2\left(U_{11}h^2a^{\star 2} + ... + 2U_{13}hla^\star c^\star\right)\right]$. For symmetry reasons the values U_{12} and U_{23} of some atoms are equal to zero in this structure.

$c = 9.11562(17)$ Å. A total of 2160 reflections (876 unique) for sample I and 3805 (1027 unique) for sample II were measured.

In the next step, we have determined the positions of the hydrogen atoms from a difference Fourier analysis. In fact, two holes were found at the positions (0.6998, 0.75, 0.0441) and (0.4273, −0.0453, 0.2233), suggesting the presence of two different hydrogen positions located at the Wyckoff positions $4c(x, 1/4, z)$ [or in the setting $(x, 3/4, z)$ given above] and $8d(x, y, z)$, respectively. For the refinements, the overall scale factor, the positional and anisotropic thermal parameters of all atoms, as well as the extinction parameter g were allowed to vary giving in total 50 parameters. The obtained residuals R_F and ωR_F are defined as $R_F = \sum (||F_{\rm obs}| - |F_{\rm cal}||) / \sum |F_{\rm obs}|$ and $\omega R_F = \sum \omega (||F_{\rm obs}| - |F_{\rm cal}||) / \sum |F_{\rm obs}|$, where $\omega = 1/\sigma^2$. The refinements finally resulted in the following residuals: $R_F = 0.107$, $\omega R_F = 0.067$ (sample I) and $R_F = 0.055$, $\omega R_F = 0.040$ (sample II). For sample I these were found to be somewhat enlarged. This can be ascribed to that the investigated crystal contains two grains, which finally resulted in a peak splitting during the measurement of particular series of Bragg reflections. However, for both samples the positional and anisotropic thermal parameters of all atoms could be determined with good accuracy. The results of the refinements are summarized in Tab. SI.

After all, the refined hydrogen positional parameters significantly differ in comparison to those obtained earlier from synchrotron powder data, whereas the parameters of the heavier atoms show a much better agreement. Here, it has to be mentioned that the positions of hydrogen atoms can be determined more precisely from neutron diffraction data. The refined extinction parameter of sample I finally resulted in $g = 275(20)\,\mathrm{rad}^{-1}$. Due to the much better crystal quality of sample II the extinction parameter $g = 2167(62)\,\mathrm{rad}^{-1}$ is strongly increased.

EXPERIMENTAL RESULTS: MAGNETIC STRUCTURE

For the investigation of the magnetic structure we used sample II. In order to determine the magnetic moments the overall scale factor has been determined from a data set collected in the paramagnetic range at 25 K (64 reflections, 35 unique). During the refinements the positional parameters and the overall scale factor were refined resulting in a residual $R_F = 0.060$ (in F). The thermal parameters and the extinction parameter were taken from the refinements of the data set collected at room temperature and were not allowed to vary.

The representation analysis was applied earlier by Bertaut [S6] to describe a series of magnetic structures. The aim is to find the basis vectors of the irreducible representations (*irreps*) contained in Γ associated with the propagation vector $\mathbf{q} = (1/2, 0, 1/2)$ in the space group *Pnma* (No. 62). The unit cell contains two magnetic Cu atoms (Cu(1) and Cu(2)) located at the Wyckoff positions $4a$ [Cu(11) $(0,0,0)$, Cu(12) $(1/2,0,1/2)$, Cu(13) $(0,1/2,0)$, Cu(14) $(1/2,1/2,1/2)$] and $4c$ [Cu(21) $(x,1/4,z)$, Cu(22) $(-x+1/2,3/4,z+1/2)$, Cu(23) $(-x,3/4,-z)$, Cu(24) $(x+1/2,1/4,-z+1/2)$]. The *irreps* and their basis functions were determined using the program *BasIreps* in the *FullProf* suite.

irrep	$\mathbf{S}_k(1)$	$\mathbf{S}_k(2)$	$\mathbf{S}_k(3)$	$\mathbf{S}_k(4)$	*irrep*	$\mathbf{S}_k(1)$	$\mathbf{S}_k(2)$	$\mathbf{S}_k(3)$	$\mathbf{S}_k(4)$
$\Gamma_1(4a)$	(u,v,w)	$i(u,v,-w)$	$(-u,v,-w)$	$i(-u,v,w)$	$\Gamma_1(4c)$	$(0,u,0)$	$i(0,u,0)$	$(0,u,0)$	$i(0,u,0)$
					$\Gamma_2(4c)$	$(u,0,v)$	$i(u,0,-v)$	$(-u,0,-v)$	$i(-u,0,v)$
$\Gamma_3(4a)$	(u,v,w)	$i(u,v,-w)$	$(u,-v,w)$	$i(u,-v,-w)$	$\Gamma_3(4c)$	$(u,0,v)$	$i(u,0,-v)$	$(u,0,v)$	$i(u,0,-v)$
					$\Gamma_4(4c)$	$(0,u,0)$	$i(0,u,0)$	$(0,-u,0)$	$i(0,-u,0)$
$\Gamma_5(4a)$	(u,v,w)	$i(-u,-v,w)$	$(-u,v,-w)$	$i(u,-v,-w)$	$\Gamma_5(4c)$	$(0,u,0)$	$i(0,-u,0)$	$(0,u,0)$	$i(0,-u,0)$
					$\Gamma_6(4c)$	$(u,0,v)$	$i(-u,0,v)$	$(-u,0,-v)$	$i(u,0,-v)$
$\Gamma_7(4a)$	(u,v,w)	$i(-u,-v,w)$	$(u,-v,w)$	$i(-u,v,w)$	$\Gamma_7(4c)$	$(u,0,v)$	$i(-u,0,v)$	$(u,0,v)$	$i(-u,0,v)$
					$\Gamma_8(4c)$	$(0,u,0)$	$i(0,-u,0)$	$(0,-u,0)$	$i(0,u,0)$

pirrep	$\mathbf{S}_k(1)$	$\mathbf{S}_k(2)$	$\mathbf{S}_k(3)$	$\mathbf{S}_k(4)$	*pirrep*	$\mathbf{S}_k(1)$	$\mathbf{S}_k(2)$	$\mathbf{S}_k(3)$	$\mathbf{S}_k(4)$
$\Gamma_1(4a)$	(u,v,w)	$(-p,-q,r)$	$(-u,v,-w)$	$(p,-q,-r)$	$\Gamma_1(4c)$	$(0,u,0)$	$(0,-v,0)$	$(0,u,0)$	$(0,-v,0)$
$\Gamma_2(4a)$	(u,v,w)	$(-p,-q,r)$	$(u,-v,w)$	$(-p,q,r)$	$\Gamma_2(4c)$	$(u,0,v)$	$(-w,0,p)$	$(u,0,v)$	$(-w,0,p)$
					$\Gamma_3(4c)$	$(u,0,v)$	$(-w,0,p)$	$(-u,0,-v)$	$(w,0,-p)$
					$\Gamma_4(4c)$	$(0,u,0)$	$(0,-v,0)$	$(0,-u,0)$	$(0,v,0)$

TABLE SII. General expressions of the Fourier coefficients $\mathbf{S}_k(j)$ obtained from the basis functions calculated from the different representations of the two Cu sites at the Wyckoff positions $4a$ (Cu(1)) [Cu(11) $(0,0,0)$, Cu(12) $(1/2,0,1/2)$, Cu(13) $(0,1/2,0)$, Cu(14) $(1/2,1/2,1/2)$] and $4c$ (Cu(2)) [Cu(21) $(x,1/4,z)$, Cu(22) $(-x+1/2,3/4,z+1/2)$, Cu(23) $(-x,3/4,-z)$, Cu(24) $(x+1/2,1/4,-z+1/2)$]. In the lower part of the table the physically irreducible representations (*pirreps*) and their Fourier components are listed.

In Tab. SII the vectors $\mathbf{S_k}(j)$ (the Fourier components of the magnetic moments) of the different *irreps* are listed. For the Cu(1) atoms located at the Wyckoff position $4a$ one finds 4 irreducible representations where the moments can be oriented along the x, y, and z directions. On the other hand, for the Cu(2) atoms, located at the Wyckoff position $4c$, one finds 4 irreducible representations, which only allow a spin alignment along the y direction, while the other 4 irreducible representations produce an alignment along the x and z directions. All *irreps* are of dimension 1. For both Cu sites it can be seen (in all *irreps*) that the coefficients of the vectors $\mathbf{S_k}(j)$ are either purely real or purely imaginary. Therefore, the *irreps* cannot describe alone real magnetic structures.

The complex basic vectors can be replaced by real ones by combining different irreducible representations (physically irreducible). The real basic functions (*Physical Irreps*) could also be determined with the program *BasIreps* in the *FullProf* suite. In the lower part of Tab. SII it can be seen that the number of irreducible representations are now reduced by a factor of 2. Due to the fact that they are now of dimension 2, each *irrep* can have two different spin sequences giving identical diffraction patterns.

In order to determine the magnetic structure, we have started to determine the moment direction and the spin sequence of the four Cu(2) atoms, which are located at the Wyckoff position $4c$. Due to the fact that the observed intensities of the magnetic reflections $(1/2\ 2\ 1/2)_\mathrm{M}$ and $(1/2\ 2\ 3/2)_\mathrm{M}$ were found to be weak we obtained the best fit if the moments are aligned parallel to the b axis. We used $\Gamma_1(4c)$ $(+\ -\ +-)$ and $\Gamma_4(4c)$ $(+\ -\ -+)$ to describe the magnetic ordering. Due to the fact that both models gave a residual of about 0.23 (in F) it was not possible to distinguish between these two models. For comparison, the refinements where we assumed a magnetic ordering within the ac plane [$\Gamma_2(4c)$ and $\Gamma_3(4c)$] resulted in a residual of about 0.42. Here, it is interesting to note that the magnetic x component is found to be zero. Accordingly, we carried out refinements where only the moments of Cu(1) (located at the Wyckoff positions $4a$) were allowed to vary. We used the spin sequences of $\Gamma_1(4a)$ and $\Gamma_2(4a)$, where the moments were allowed to vary along the axes x, y, and z. We have obtained a better fit for $\Gamma_1(4a)$ than for $\Gamma_2(4a)$ resulting in the residuals 0.24 and 0.32, respectively. Again, it is interesting to note that the x component for $\Gamma_1(4a)$ is also found to be zero. These results are in agreement with the magnetization measurements, where the a axis was found be the hard axis of the magnetization.

Several trials showed that only one model gave a satisfactory fit reaching a residual $R_M = 0.107$ (in F), where we used $\Gamma_1(4c)$ for Cu(2) $(+\ -\ +-$ along $y)$ and $\Gamma_1(4a)$ for Cu(1) $(+\ -\ -+$ along x, $+\ -\ +-$ along y, and $+\ +\ --$ along $z)$. Interestingly, the refinements caused a spin inversion of the Cu(1) atoms $(-\ +\ +-$ along x, $-\ +\ -+$ along y, and $-\ -\ ++$ along $z)$. This means that the exchange interactions between the atoms Cu(11) in $(0, 0, 0)$ and Cu(21) in $(0.1907, 1/4, 0.2553)$ are antiferromagnetic. This is unusual since the moments of Cu(2) are aligned parallel to the b direction, and the moments of Cu(1) predominantly parallel to the c direction.

For the refinement of the magnetic structure at 2.2 K, we used 10 magnetic reflections where the nuclear contribution is negligible. The observed and calculated magnetic intensities of the reflections are listed in Tab. SIII. The magnetic components of Cu(1) are $\mu_{\mathrm{ord,Cu(1)}}(x) = 0.09(9)\,\mu_\mathrm{B}$, $\mu_{\mathrm{ord,Cu(1)}}(y) = 0.04(2)\,\mu_\mathrm{B}$ and $\mu_{\mathrm{ord,Cu(1)}}(z) = 0.32(7)\,\mu_\mathrm{B}$, giving a total moment $\mu_{\mathrm{ord,Cu(1)}} = 0.34(4)\,\mu_\mathrm{B}$. For the Cu(2) atom, where only a y component could be found, the moment is $\mu_{\mathrm{ord,Cu(2)}} = \mu_{\mathrm{ord,Cu(2)}}(y) = 0.59(2)\,\mu_\mathrm{B}$. Altogether, the resulting complex magnetic structure is visualized in Fig. 1 (b) in the main text and in Fig. S1.

$(hkl)_\mathrm{M}$	F^2_obs	F^2_cal	ΔF^2
(1/2 0 1/2)	38.8	36.5	2.3
(1/2 1 1/2)	28.6	27.6	1.0
(1/2 0 3/2)	48.5	47.7	0.8
(1/2 1 3/2)	12.8	13.2	−0.4
(3/2 0 1/2)	30.9	37.8	−6.9
(1/2 0 5/2)	53.3	35.9	−7.4
(3/2 1 1/2)	52.7	51.0	1.7
(3/2 0 3/2)	19.2	28.0	−8.8
(1/2 2 1/2)	1.4	3.8	−2.4
(1/2 1 5/2)	44.2	48.1	−3.9
(3/2 1 3/2)	41.5	38.9	5.6
(1/2 2 3/2)	1.6	7.3	−5.7
(3/2 0 5/2)	21.3	30.0	−8.7

TABLE SIII. Calculated and observed intensities (given as F^2) of atacamite $Cu_2Cl(OH)_3$ obtained from the refinement of the magnetic structure at 2.2 K resulting in a residual of $R_M = 0.107$ (in F). Symmetry equivalent reflections were averaged.

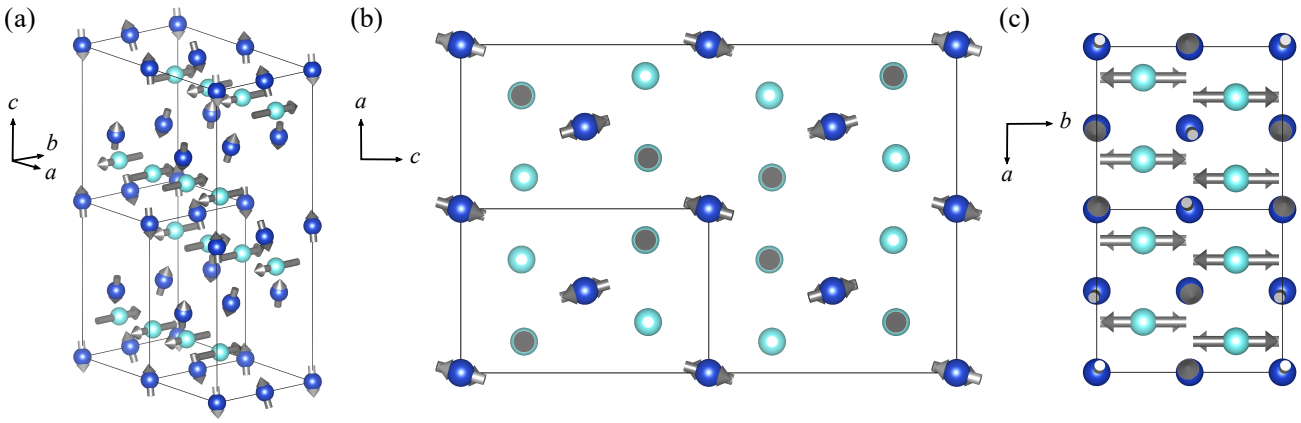

FIG. S1. (color online) Magnetic structure of atacamite $Cu_2Cl(OH)_3$ obtained from single crystal neutron diffraction experiments (a) with additional views along the b axis (b) and the c axis (c). The black solid lines represent the nuclear and the magnetic unit cell; for details see text.

EXPERIMENTAL RESULTS: HEAT CAPACITY AND ENTROPY

We estimate the magnetic entropy of atacamite by calculating $S_{\rm mol} = \int c_p/T \; dT$ from our heat capacity data at 0 T (see Fig. S2). We ignore the phonon contribution for our estimation. Since the experimental data were measured down to a temperature of 2 K, for the evaluation of $S_{\rm mol}$, the low-temperature heat capacity was approximated for the integration using an exponential function $\sim \exp(-\Delta/T)$ (gray data points in Fig. S2). This calculation yields a value of $S_{\rm mol} \sim 0.65 R \ln 2$ at $T_{\rm N} = 8.4$ K.

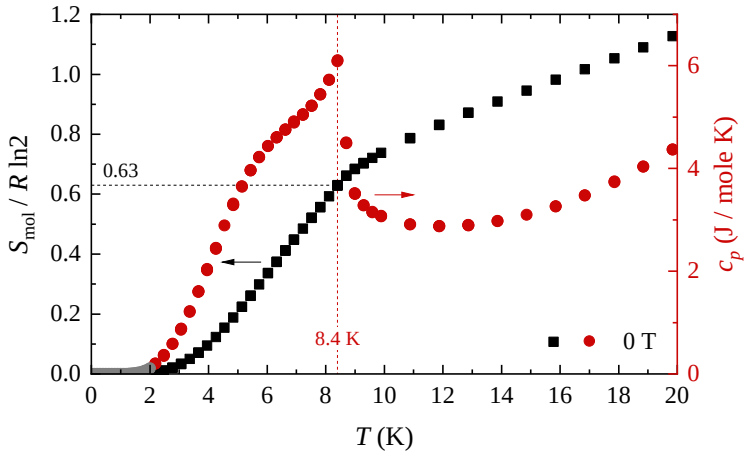

FIG. S2. (color online) Heat capacity c_p and entropy $S_{\rm mol}$ of atacamite $Cu_2Cl(OH)_3$; for details see text.

THEORETICAL RESULTS: ELECTRONIC STRUCTURE AND ENERGY MAPPING

We performed electronic structure calculations for acatamite in the above-described orthorhombic *Pnma* structure. We use the parameters of Ref. [S5] determined by X-ray diffraction performed on natural atacamite crystals. Note that the crystal structure from Ref. [S5] has highly unlikely hydrogen positions with OH distances of 1.67 Å or more. Therefore, we first relaxed the hydrogen positions (while fixing lattice parameters and all other positions to the values given by Ref. [S5]). The resulting positions for H(1): (−0.3076, 3/4, 0.0388) and H(2): (0.4237, −0.4477, 0.2214) are much closer to the values independently determined in our neutron diffraction refinement.

bond	length (Å)	sites connected	comment
J_1	3.01552	Cu(2)-Cu(2)	
J_2	3.11134	Cu(1)-Cu(2)	symmetric
J_3	3.37616	Cu(1)-Cu(2)	in-chain
J_4	3.43192	Cu(1)-Cu(1)	in-chain
J_5	5.02492	Cu(1)-Cu(2)	symmetric (small)
J_6	5.46421	Cu(1)-Cu(1)	(small)
J_7	5.67145	Cu(1)-Cu(2)	symmetric (small)
J_8	5.75017	Cu(2)-Cu(2)	(small)
J_9	5.76511	Cu(1)-Cu(2)	symmetric
J_{10}	5.91223	Cu(1)-Cu(2)	symmetric
J_{11a}	6.02795	Cu(1)-Cu(1)	(small)
J_{11b}	”	Cu(2)-Cu(2)	
J_{12}	6.07949	Cu(2)-Cu(2)	(small)
J_{13}	6.22269	Cu(2)-Cu(2)	
J_{14}	6.45257	Cu(1)-Cu(1)	(small)
J_{15}	6.75231	Cu(2)-Cu(2)	in-chain
J_{16}	6.86383	Cu(1)-Cu(1)	in-chain
J_{17}	6.88152	Cu(2)-Cu(2)	omitted

TABLE SIV. Classification of exchange couplings of atacamite up to the third nearest neighbour sphere in the distorted pyrochlore lattice. The effective 3D Hamiltonian is formed by couplings of Cu(2)-Cu(2) connectivity.

As discussed in the main text, this structure may be viewed as a distorted pyrochlore structure, so there are 18 inequivalent bonds with the length under 7 Å (see Tab. SIV). These naturally fall into three groups that are offsprings of the three nearest neighbor shells in the pyrochlore parent, namely J_{1-4}, J_{5-10} and J_{11-17}, respectively (note that J_{11a} and J_{11b} have the same length, but are crystallographically different). According to the calculations (see results in Tab. SV and Fig. S3), the two parameters $J_{3,4}$ are one to two orders of magnitude stronger than everything else, which allows us to separate the problem into two different energy scales: one describing the spin dynamics inside a Δ-chain and the other describing the interactions between the chains. The same separation allows us to neglect all interactions between the spins in the same chain (marked as “in-chain” in the Tab. SIV) except those two.

We furthermore neglect inter-chain interactions that cancel out nearly exactly because of the AFM ordering of the Cu(1) spins inside each chain (“symmetric” in Tab. SIV). Finally, we left out J_{17} because it is the longest-range interaction and would require additional doubling of the supercell used for all other calculations. This leaves us with

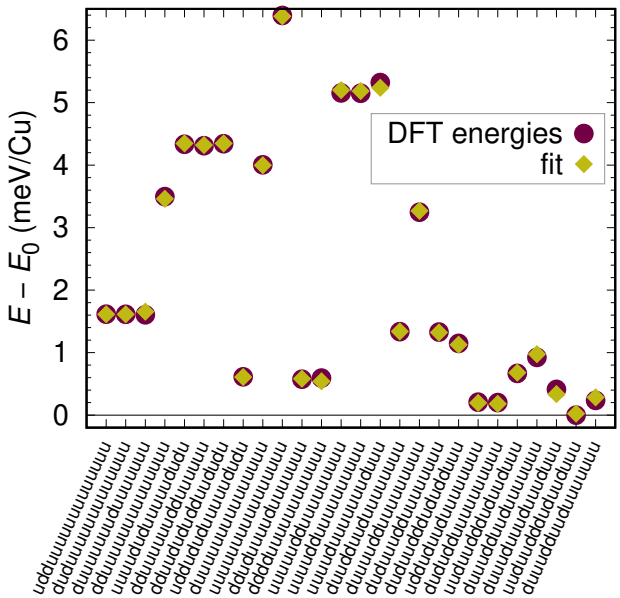

FIG. S3. Comparison between GGA+U, $U = 8\,\mathrm{eV}$, $J_\mathrm{H} = 1\,\mathrm{eV}$ total energies (per Cu^{2+}) for $Cu_2Cl(OH)_3$ and the energies calculated from the Heisenberg Hamiltonian with the ten exchange couplings.

U (eV)	J_1 (K)	J_2 (K)	J_3 (K)	J_4 (K)	J_5 (K)	J_6 (K)	J_7 (K)	J_8 (K)
7	20.(1.5)	−7.1(1.8)	128.0(1.2)	411.5(8)	0.4(9)	0.8(9)	0.3(1.1)	−0.1(6)
7.5	11.9(1.3)	−8.3(1.6)	116.7(1.1)	379.6(7)	0.3(8)	0.6(7)	0.3(1.0)	−0.1(5)
8	4.5(1.0)	−9.2(1.2)	106.3(8)	349.5(6)	0.2(6)	0.5(6)	0.3(7)	0.0(4)
8.24	**1.3(9)**	**-9.6(1.1)**	**102.0(7)**	**336.0(6)**	**0.2(6)**	**0.4(6)**	**0.3(7)**	**0.0(4)**
8.5	−2.0(8)	−9.9(1.0)	96.8(6)	321.3(5)	0.1(5)	0.3(5)	0.3(6)	0.0(3)
d_{Cu} (Å)	3.016	3.121	3.365	3.432	5.032	5.464	5.664	5.747

U (eV)	J_{11a} (K)	J_{11b} (K)	J_{12} (K)	J_{13} (K)	J_{14} (K)	θ_{CW} (K)
7	−0.4(6)	19.4(9)	−0.1(9)	−1.5(9)	−0.5(5)	−173
7.5	−0.3(5)	17.8(8)	−0.1(1.0)	−1.3(8)	−0.4(4)	−156
8	−0.2(4)	16.3(6)	−0.1(6)	−1.2(6)	−0.3(3)	−141
8.24	**−0.2(4)**	**15.6(6)**	**−0.1(6)**	**−1.1(6)**	**−0.3(3)**	**−134**
8.5	−0.2(3)	14.9(5)	−0.1(4)	−1.1(5)	−0.2(3)	−127
d_{Cu} (Å)	6.028	6.028	6.079	6.24146	6.45258	

TABLE SV. Exchange couplings of atacamite $Cu_2Cl(OH)_3$ determined by energy mapping. The Hund rule coupling was fixed at $J_{\mathrm{H}} = 1\,\mathrm{eV}$. A $\sqrt{2} \times 1 \times \sqrt{2}$ supercell was used. The line in bold face marks the interpolated set of couplings that yields the experimental Curie-Weiss temperature.

six parameters, shown in Fig. S4.

THEORETICAL RESULTS: CLASSICAL MEAN FIELD THEORY OF AN INDIVIDUAL Δ-CHAIN AND A COLLECTION OF CHAINS

In the following, we will consider the classical ground state expected for a J, J' Δ-chain with antiferromagnetic J and J'. As J and J' are much larger than the other exchange couplings determined for atacamite, we will subsequently assume this ground state spin configuration to be rigidly frozen at $T = 0$ and determine how the effective magnetic moments of the Δ-chain are tilted by the application of a magnetic field.

As a first step, we consider a single Δ-chain as depicted in Fig. S5 (a). The angles that the four moments in the

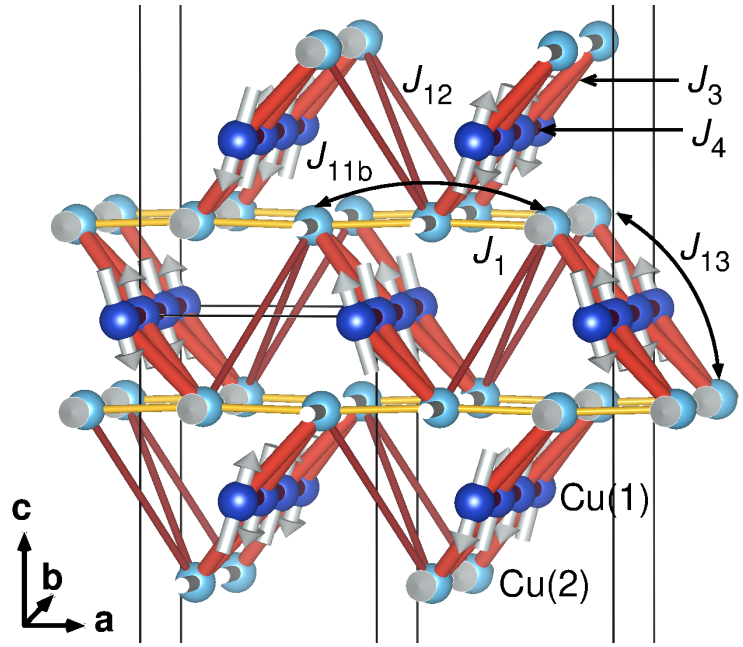

FIG. S4. Cu lattice of atacamite $Cu_2Cl(OH)_3$ with the exchange paths which are active in the tilting of the ground state magnetic moments in a magnetic field **H**.

translational unit form with the b axis are denoted as α, α', β and β'. We use the notation for the interactions as introduced for atacamite in Fig. 1 of the main text. The coupling between Cu(1) atoms along the chain is $J \equiv J_4$ where $J_4 = 336\,\mathrm{K}$, the coupling between Cu(1) and Cu(2) is $J' \equiv J_3$ where $J_3 = 102\,\mathrm{K}$. We will normalize to a single Cu site and first calculate the energy E per Cu:

$$\begin{aligned} 4E &= 2J\mathbf{S}_1 \cdot \mathbf{S}'_1 + J'(\mathbf{S}_1 \cdot \mathbf{S}_2 + \mathbf{S}_2 \cdot \mathbf{S}'_1 + \mathbf{S}'_1 \cdot \mathbf{S}'_2 + \mathbf{S}'_1 \cdot \mathbf{S}_2) \\ &= 2J\cos(\alpha - \alpha') + J[\cos(\alpha - \beta) + \cos(\alpha' - \beta) \\ &\qquad + \cos(\alpha' - \beta') + \cos(\alpha - \beta')] \end{aligned} \tag{S1}$$

Without spin orbit coupling, the spin space is rotationally invariant, so we can impose one directional constraint. We choose $\alpha' = -\alpha$. Then

$$\begin{aligned} 4E &= 2J\cos 2\alpha + J'[\cos(\alpha - \beta) + \cos(\alpha + \beta) \\ &\qquad + \cos(\alpha - \beta') + \cos(\alpha + \beta')] \\ &= 2J\cos 2\alpha + 2J'[\cos\alpha\cos\beta + \cos\alpha\cos\beta'] \end{aligned} \tag{S2}$$

Minimizing this with respect to β and β' we see right away that $\beta = \beta' = 0$. Using this we have

$$2E = J\cos 2\alpha + 2J'\cos\alpha \tag{S3}$$

which we minimize with respect to α:

$$J\sin 2\alpha + J'\sin\alpha = 0 \tag{S4}$$

This yields the equilibrium canting angle

$$\alpha = \cos^{-1}\left(-\frac{J'}{2J}\right). \tag{S5}$$

If $J' = 0$, the Cu(1) form a perfect Néel chain, if $J' = J$, $\alpha = 2\pi/3 = 120°$, and if $J' \geq 2J$, the Cu(1) spins are aligned along b. With the values $J' = 102$ K and $J = 336$ K, this means $\alpha \approx 98.7°$ (see Fig. S5 (b)). Note that this angle $\alpha \approx 98.7°$ means that the projection of the $\mathbf{S}_1$ moment on the b axis is $\propto \cos\alpha = -0.152$, *i.e.* it is opposed to the $\mathbf{S}_2$ moment, in agreement with the antiferromagnetic coupling J_3.

We start with the classical ground state expected for a J, J' Δ-chain with antiferromagnetic J and J'. As J and J' are much larger than the other exchange coupling determined for atacamite, we will subsequently assume this ground state spin configuration to be rigidly frozen at $T = 0$ and determine how the effective magnetic moments of the Δ-chain are tilted by the application of a magnetic field.

Before proceeding, we make two observations. First, Heisenberg interchain interactions involving Cu(1) effectively cancel out. Indeed, neighboring Δ-chains are staggered by half a translational unit, so any spin that interacts with a Cu(1) in a given neighboring Δ-chain will also interact with another Cu(1) that has an opposite spin. Given that the very strong Cu(1)-Cu(1) intrachain interactions keep the Cu(1) chain approximately antiferromagnetic, these two interactions almost cancel out ("symmetric" in Tab. SIV). Moreover, Cu(1) and Cu(2) spins are nearly

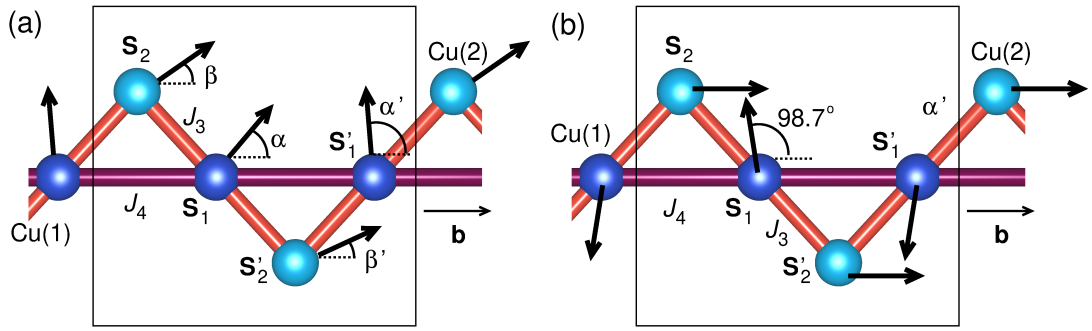

FIG. S5. (a) Notations to fix the classical ground state of the Δ-chain. The rectangle indicates the translational unit. (b) Ground state spin structure found in atacamite, using the calculated exchange coupling values.

orthogonal, so any interchain Heisenberg interaction of that kind (like J_2 and J_7) is multiplied by a factor of the order of $\cos 98.7^\circ = -0.152$. We neglect all these interactions, as well as interactions marked "small" in the Tab. SIV, which are numerically less than 1 K, and combine the remaining interactions into $J_A = J_1/2 + J_{13}/2$, $J_B = J_1/2$, $J_C = J_{11b}/2 + J_{12}/2$ where factors 1/2 ensure counting interaction per Cu even though the couplings involve only Cu(2). However, for consistency we neglect J_{12} in this formula as it is too small to be calculated reliably (see Table SV). The resulting A, B, C triangular lattice is shown in the inset of Fig. S6 (a).

Next, we replace each Δ-chain with a single classical magnetic object with $M_{\rm eff}$ per Cu calculated as

$$M_{\rm eff}(H) = \frac{M_1(H)\cos\alpha + M_2(H)}{2} = \frac{M_2(H)}{2} - \frac{J' M_1(H)}{4J}. \tag{S6}$$

where $M_{1,2}$ are effective (fluctuation-reduced) magnetic moments on the corresponding Cu sites. As discussed in the main text, the moments in $H = 0$ are known from the experiment to be $M_1(0) = 0.34\,\mu_B$ and $M_2(0) = 0.59\,\mu_B$, so that $M_{\rm eff}(0) = 0.27\,\mu_B$. In a sufficiently high field these fluctuations are suppressed, in the first approximation linearly [S7], so that the moments become $M_1 = M_2 = 1\,\mu_B$ again. In this field, $M_{\rm eff}(H_{\rm sat}) = (1/2 - J'/4J)\,\mu_B = 0.42\,\mu_B$. The latter number agrees very well with the experimental value at the plateau, so we conclude that the plateau field $H_2 \approx H_{\rm sat}$. With this in mind, we take

$$\begin{aligned} M_1(H) &\approx \left(0.34 + 0.66\frac{H}{H_2}\right)\mu_B \\ M_2(H) &\approx \left(0.59 + 0.41\frac{H}{H_2}\right)\mu_B \\ M_{\rm eff}(H) &\approx \left(0.27 + 0.15\frac{H}{H_2}\right)\mu_B \end{aligned} \tag{S7}$$

Note that in this derivation we assumed that the effective magnetic moments are suppressed by the fluctuations, but the exchange interactions are not. Another choice would be to write the effective interations as $J_i \mathbf{M}\cdot\mathbf{M}'/4$ (the factor of 1/4 accounting for the electron g-factor), in which case J and J' in Eq. (S6) should be replaced by $J_{\rm eff}(H) = JM_1^2(H)/(4\,\mu_B^2)$ = and $J'_{\rm eff}(H) = J'M_1(H)M_2(H)/(4\,\mu_B^2)$ so that $J'_{\rm eff}(H)/J_{\rm eff}(H) = J'M_2(H)/JM_1(H)$, and

$$\begin{aligned} M_{\rm eff}(H) &= \frac{M_2(H)}{2} - \frac{J'M_1(H)}{4J}\frac{M_2(H)}{M_1(H)} = M_2(H)\left(\frac{1}{2} - \frac{J'}{4J}\right) \\ &= 0.42 M_2(H) \approx \left(0.25 + 0.17\frac{H}{H_2}\right) \end{aligned} \tag{S8}$$

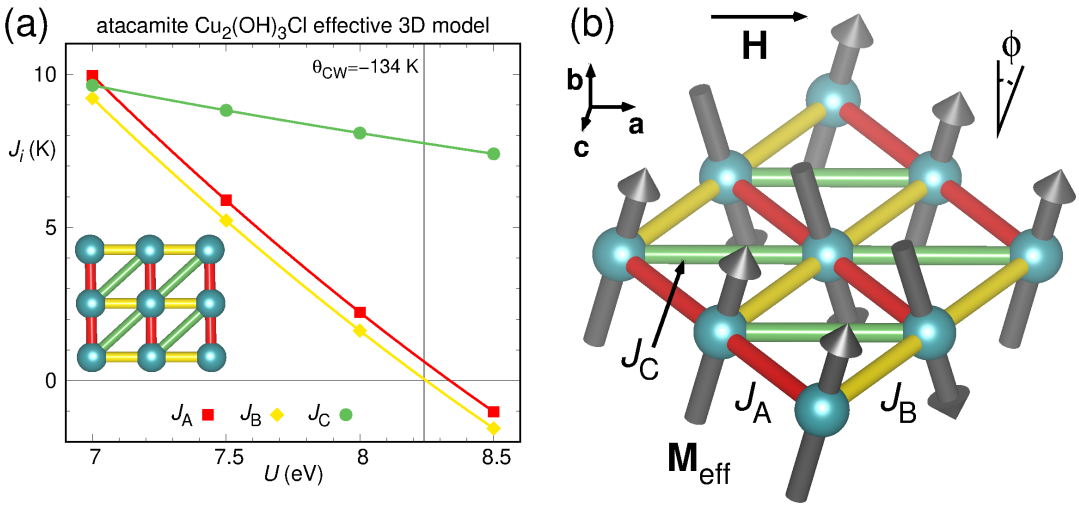

FIG. S6. (a) Effective three-dimensional couplings for atacamite. The inset shows the fully anisotropic triangular lattice formed by the three effective couplings J_A, J_B and J_C. (b) Illustration of the effective model for atacamite in the ac plane, obtained by assuming a fixed effective moment $M_{\rm eff}$ for the strongly coupled Δ-chains. The magnetic order observed by neutrons implies a stripe order of the effective spin and coincides with the classical ground state of the J_A-J_B-J_C model determined in (a).

Barring a microscopic theory, it is hard to chose one approximation over the other. We will use the latter in the rest of the paper, but qualitatively the results are the same.

Upon replacing each Δ-chain with one classical moment $M_{\rm eff}(H)$, we have a model equivalent, in MFA, to a classical 2D triangular lattice Heisenberg model, with three different exchange couplings, with one of them, $J_{\rm C}$, dominant. The ground state is a linear AFM Néel chain in $J_{\rm C}$ direction, ferromagnetically aligned along $J_{\rm A}$. The situation is illustrated in Fig. S6 (b). There, each sphere represents a Δ-chain along b with effective moment $M_{\rm eff}$ per Cu, and the red, yellow and green bonds are the interchain interactions. Since $J_{\rm B} \lesssim J_{\rm A} \ll J_{\rm C}$, we leave only the latter, replacing it with $J_{\Delta-\Delta} \gtrsim J_{\rm C}$, absorbing all interactions in one parameter. The problem is then reduced to a 1D AF chain with the Heisenberg energy $J_{\Delta-\Delta}M^2_{\rm eff}(H)\cos\theta/4$, where θ is the angle between the net moment of the two Δ-chains connected by $J_{\Delta-\Delta}$. We now write the total energy of the system in an external field **H** as

$$\begin{aligned} E &= -M_{\rm eff}(H)H\sin\phi - \frac{1}{4}J_{\Delta-\Delta}M_2^2(H)\cos 2\phi + E_{\rm aniso} \\ E_{\rm aniso} &= K\cos^2\phi \end{aligned} \tag{S9}$$

where ϕ is the canting angle towards **H** (note that the $J_{\Delta-\Delta}$ interaction is only between Cu(2); therefore, only $M_2(H)$ enters the Heisenberg term; Heisenberg interaction for Cu(2) is $2J_{\Delta-\Delta}$ but counting of the Hamiltonian per Cu means another factor 1/2). Minimizing the energy without the small anisotropic term with respect to ϕ, we get

$$\begin{aligned} \sin\phi &= HM_{\rm eff}(H)/M_2^2(H)J_{\Delta-\Delta} \\ E(H) &= -\frac{1}{4}J_{\Delta-\Delta}M_2^2(H) - H^2M_{\rm eff}^2(H)/2M_2^2(H)J_{\Delta-\Delta}. \end{aligned} \tag{S10}$$

If the field is applied along the easy axis, as it is in the experiment, the classical spin flop occurs at the $H_{\rm sf}$ such that $|E(H_1)| = E_{\rm aniso}$, so $H_{\rm sf} \approx \frac{M_2(0)}{M_{\rm eff}(0)}\sqrt{2J_{\Delta-\Delta}K}$. Taking the experimental value $H_{\rm sf} = 3.5$ T, and the calculated value $J_{\Delta-\Delta} \approx J_{\rm C} + J_{\rm B} \approx 8.5$ K, we get $K \sim 0.04$ K.

Now, neglecting the small anisotropy term, we calculate the total magnetization as a function of field:

$$\begin{aligned} M_{\rm total} &= M_{\rm eff}(H)\sin\phi = HM_{\rm eff}^2(H)/M_2^2(H)J_{\Delta-\Delta} \\ &= \frac{H}{12.7}\frac{\left(0.27+0.15\frac{H}{H_2}\right)^2}{\left(0.59+0.41\frac{H}{H_2}\right)^2}\,\frac{\mu_{\rm B}}{\rm T} \end{aligned} \tag{S11}$$

Note that 8.5 K is equivalent to 12.7 T. This expression agrees well with the experiment (see Fig. 3 (d) in the main text), and gives the "plateau" field H_2, defined in such a way that the magnetic moment at $H = H_2$ is 0.42 $\mu_{\rm B}$ to be 30.1 T, to be compared to the experimental number of 31.5 T.

We can also consider the plateau regime itself. Its slope is determined by the energy balance inside an individual Δ-chain in an external field. We need to modify Eq. (S3) to account for the Zeeman energy (note that the Cu magnetic moments at this point are already quenched to 1 $\mu_{\rm B}$):

$$2E = J\cos 2\alpha + 2J'\cos\alpha - 2M_{\rm eff}H \tag{S12}$$

$$= J\cos 2\alpha + 2J'\cos\alpha - (1+\cos\alpha)\mu_{\rm B}H \tag{S13}$$

After minimization, we find that now instead of $M_{\rm eff} = (1/2 - J'/4J)\,\mu_{\rm B} = 0.42\,\mu_{\rm B}$, we get $M_{\rm eff} = (1/2 - J'/4J + H/4J)\,\mu_{\rm B} = 0.42\,\mu_{\rm B} + (0.0007\,\mu_{\rm B}/{\rm T})H$. This is nearly an order of magnitude too small (the experimental number is $0.0022\,\mu_{\rm B}/{\rm T}$), but it is qualitatively correct.

EXPERIMENTAL RESULTS: METAMAGNETIC TRANSITION

The magnetization measurements with the magnetic field **H** aligned along the b axis reveal a complex metamagnetic transition (see Fig. S7 (a)). While at temperatures up to $T \sim 6$ K there is a two-step transition, at higher temperatures only a single transition is observed. Magnetic hysteresis arises because of the pulsed field character of the measurement. The metamagnetic transition can also be found in the low-field magnetostriction data after smoothing of the data (see Fig. S7 (b)). Here, a shallow minimum in $\Delta L/L$ appears at the upper field of the two-step transition.

This type of metamagnetic transition is consistent with the magnetic structure (see Fig. S1), with the easy magnetic axis for the larger magnetic moment on the Cu(2) ions being the b axis. Possibly, the two-step transition reflects that

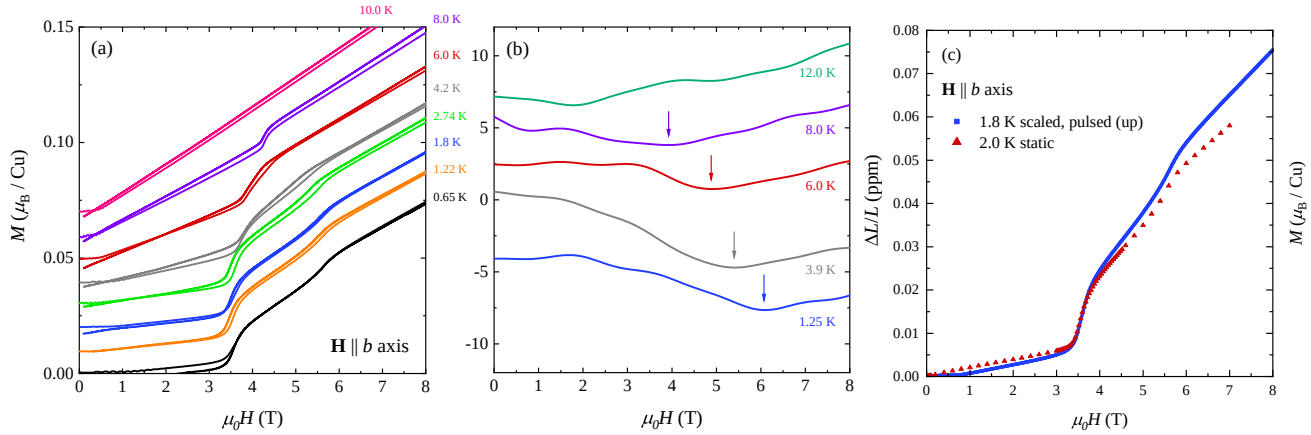

FIG. S7. (color online) The magnetization of atacamite $Cu_2Cl(OH)_3$ at low fields $\mathbf{H} \parallel b$ axis and temperatures between 0.65 and 10 K. The magnetization data for temperatures $T > 0.65$ K were shifted along the vertical axis by an offset of $+0.01\,\mu_B$ / Cu respectively (a). The metamagnetic transition can also be found in the low-field magnetostriction data (smoothed) (b). In (c), the magnetization measured at $T = 1.8$ K in pulsed magnetic fields (pulse-field up only) is shown together with a magnetization measured in a SQUID magnetometer at $T = 2.0$ K; for details see text.

the Cu(1) ions also undergo a metamagnetic transition, eventually at slightly different (higher) fields, following the Cu(2) ions.

In Fig. S7 (c), we present the low-field region of the magnetization measured at $T = 1.8$ K in pulsed magnetic fields (pulse-field up only) together with a magnetization measured in a SQUID magnetometer at $T = 2.0$ K. The metamagnetic transition is observed by both techniques.

THEORETICAL RESULTS: EXACT DIAGONALIZATION FOR THE SAWTOOTH CHAIN WITH IN-CHAIN FRUSTRATION

The reduced magnetic moments that are measured along the chain axis could suggest the existence of an additional degree of frustration in the system. To investigate such a scenario, we have studied the sawtooth chain in the presence of an additional, in-chain, next-nearest-neighbor coupling (NNN) J_f as depicted in Fig. S8 using full diagonalization and the Lanczos algorithm for system sizes up to $L = 28$ spins. The Hamiltonian of the system reads

$$H = \sum_{i=\text{even}} \left(J\mathbf{S}_i \cdot \mathbf{S}_{i+2} + J_f \mathbf{S}_i \cdot \mathbf{S}_{i+4}\right) + \sum_i \left(J'\mathbf{S}_i \cdot \mathbf{S}_{i+1} - hS_i^z\right). \tag{S14}$$

In finite systems with L spins, the magnetization will necessarily display quantization steps of minimum distance $2/L$. Connecting the middle point of these steps would provide a good estimate for the magnetization curve in the thermodynamic limit [S8]. In Fig. S9, we present the magnetization vs. the magnetic field for the system described by the Hamiltonian in Eq. (S14). We fix the J' coupling to $J' = 2J$, which ensures the maximum magnetization plateau at half saturation, $M = M_{\text{sat}}/2$, with $M_{\text{sat}} = L/2$, for a vanishing J_f [S9]. For $J_f = 0$, the plateau at $M = M_{\text{sat}}/2$ extends from $h \simeq 2.9J$ up to $h \simeq 4J$, after which it jumps directly to the saturation value M_{sat}. As the NNN coupling

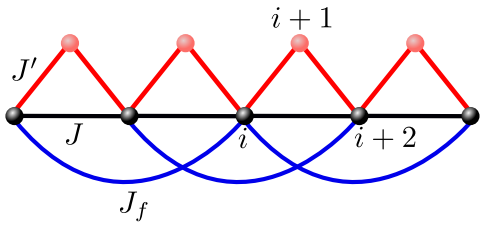

FIG. S8. The sawtooth chain in the presence of an additional in-chain NNN frustrating coupling. Neighboring spins along the chains are coupled via J, while the NNN ones via J_f. Finally, spins are also coupled in the sawtooth pattern via J'.

is switched on, the magnetization plateau shrinks with increasing J_f. The same behavior is observed for other values of the ratio J'/J, which strongly suggests that an in-chain frustration as described by the Hamiltonian in Eq. (S14) would reduce the size of a magnetization plateau and not stabilize it.

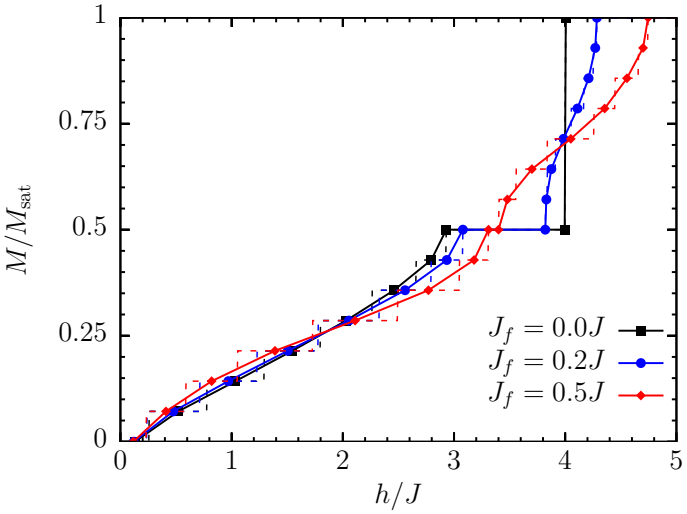

FIG. S9. Zero-temperature magnetization versus the magnetic field for $J' = 2J$ and $J_f/J = 0.0$, 0.2, 0.5 for a system of $L = 28$ sites, evaluated using full and Lanczos diagonalization. The magnetization axis is normalized with the saturation value $M_{\rm sat} = L/2$. Solid lines should give an estimate of the magnetization curve in the thermodynamic limit, while dashed lines depict the actually computed magnetization curve.

THEORETICAL RESULTS: EXACT DIAGONALIZATION FOR A SAWTOOTH CHAIN AT WEAK J'/J

Here, we briefly comment on our results from zero-temperature exact diagonalization (ED) of the Δ-chain. We have evaluated the magnetization in the low-field regime using ED on up to $L = 28$ sites at small $J'/J = 0.33$. The results are shown in Fig. S10. With ED, one must not break a continuous symmetry, because of the finite system size. More precisely, in terms of the limits discussed in the main text, $\lim_{h\to 0}\langle S^z\rangle(L, h, T) = 0$ for any finite L and T. This is certainly true in Fig. S10. However, this figure also encodes another information, which can be extracted considering the finite but small field $h^\star(L)$, roughly set by the edge of the jump to the flat region, developing at $M_0(L) \sim 0.43$ as L increases. The specific value of $h^\star(L)$ is dictated by details of the level spacings. With this, Fig. S10 strongly

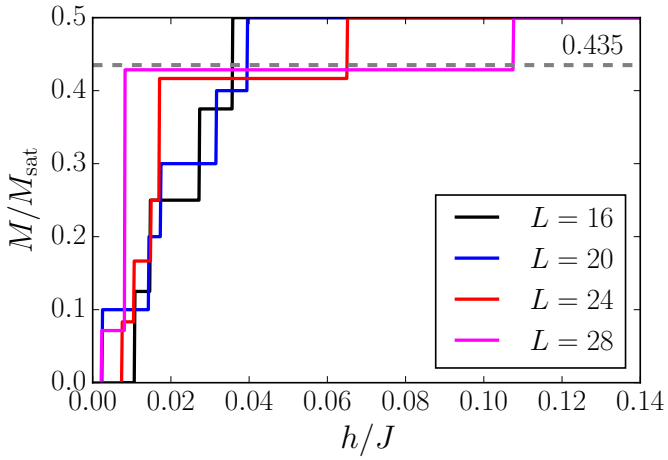

FIG. S10. Low-field magnetization of the Δ-chain normalized to the saturation value, at zero temperature, for $J'/J = 0.33$, and for different system sizes L, obtained via ED.

suggests that $(h^\star(L), M_0(L)) \to (0, \sim 0.43)$, as $L \to \infty$. *I.e.*, while accepting the limitations of small system sizes, ED is consistent with SU(2) symmetry breaking in the thermodynamic limit at $T = 0$. Conceptually, this agrees with the conclusions from iTEBD in the main text. Regarding the value of the ordered moment for the J'/J selected, it is in line with the iTEBD and the classical analysis.

REFERENCES

[S1] S. R. Hall, G. S. D. King, J. M. Stewart, Eds., *Xtal* 3.4 User's Manual. University of Australia: Lamb, Perth (1995).

[S2] V. F. Sears, in *International Tables for Crystallography*, ed. by A. J. C. Wilson (Kluwer Academic Publishers, Dordrecht/Boston/London, 1995), Vol. C, p. 383.

[S3] P. J. Brown, in *International Tables for Crystallography*, ed. by A. J. C. Wilson (Kluwer Academic Publishers, Dordrecht/Boston/London, 1995), Vol. C, p. 391.

[S4] L. Heinze, R. Beltran-Rodriguez, G. Bastien, A. U. B. Wolter, M. Reehuis, J.-U. Hoffmann, K. C. Rule, and S. Süllow, The magnetic properties of single-crystalline atacamite, $Cu_2Cl(OH)_3$, Physica B **536**, 377 (2018).

[S5] X. G. Zheng, T. Mori, K. Nishiyama, W. Higemoto, H. Yamada, K. Nishikubo, and C. N. Xu, Antiferromagnetic transitions in polymorphous minerals of the natural cuprates atacamite and botallackite $Cu_2Cl(OH)_3$, Phys. Rev. B **71**, 174404 (2005).

[S6] E. F. Bertaut, Representation analysis of magnetic structures, Acta Cryst. A **24**, 217 (1968).

[S7] M. E. Zhitomirsky and T. Nikuni, Magnetization curve of a square-lattice Heisenberg antiferromagnet, Phys. Rev. B **57**, 5013 (1998).

[S8] A. Metavitsiadis, C. Psaroudaki, and W. Brenig, Enhancement of magnetization plateaus in low-dimensional spin systems, Phys. Rev. B **101**, 235143 (2020).

[S9] J. Richter, O. Derzhko, A. Honecker, The sawtooth chain: From Heisenberg spins to Hubbard electrons, Int. J. Modern Phys. B **22**, 4418 (2008).